ACS Sustainable Chemistry & Engineering

pubs.acs.org/journal/ascecg

Research Article

Ultrafast Formation of Carbon Dioxide Hydrate Foam for Carbon Sequestration

Awan Bhati, Mark Hamalian, Palash V. Acharya, and Vaibhav Bahadur*

Cite This: https://doi.org/10.1021/acssuschemeng.4c03809

Read Online

ACCESS | Metrics & More | Article Recommendations | Supporting Information

ABSTRACT: We report ultrafast formation of carbon dioxide (CO_2) hydrate foam without the use of any conventional chemical promoters or mechanical agitation. Our 6× enhancement in the CO_2 sequestration rate (based on net gas consumption) results from the high flow rate sparging of CO_2 gas in water in an open system (constant gas inflow/outflow) in the presence of magnesium. This approach continuously renews the gas−water−hydrate interface, thereby increasing the growth rate. The CO_2 gas consumption rate (for hydrate foam formation) and foam composition (hydrate, CO_2 dissolved in water, trapped CO_2 gas) are experimentally quantified versus various parameters, including thermodynamic (pressure), CO_2 flow-related parameters (flow rate, duration), water composition, and quantity of magnesium. The maximum measured CO_2 sequestration rate (time-averaged) of 1276.5 g h^{-1} L^{-1} MPa^{-1} is 6 times higher than the fastest reported instantaneous rate. Importantly, we show rapid foam formation with saltwater, which will greatly improve the techno-economics. We develop an analytical framework to evaluate the composition of foam. We discover that the reactor pressure is a key determinant of the sequestration rate under high flow rate conditions, with magnesium playing a catalytic role. Overall, such foams enable new approaches to transport and sequester CO_2 and benefit other applications that are hindered by notoriously sluggish hydrate formation.

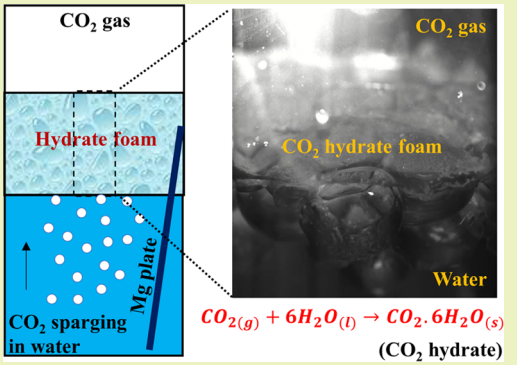

KEYWORDS: *carbon dioxide hydrates, carbon capture and sequestration, magnesium, bubble column reactor, hydrate nucleation, hydrate growth kinetics*

INTRODUCTION

There is broad consensus among the global scientific community that gigascale carbon capture and sequestration (CCS) will be imperative to mitigate the negative impacts of climate change in view of the slow pace of decarbonization.[1] CCS requirement estimates by 2050 exceed 10 Gigatons/yr.[1,2] In contrast, existing global CCS capacity in 2020 was <50 Megatons/yr.[1] Clearly, huge opportunities exist for an array of CCS technologies across various regions. Commensurate with these opportunities is the expansion of research into frontier areas such as direct air capture, ocean water capture, etc.

This study focuses on a nonconventional approach for the sequestration of carbon dioxide (CO_2). The state-of-the-art sequestration technique is the injection of CO_2 in reservoirs. However, there are limited reservoirs[3] that have permits for long-term sequestration. Currently, only 2 Class VI wells exist in the US, which allow injection for long-term sequestration; all other injection projects are associated with enhanced oil recovery.[4] Reasons for limited reservoirs and slow permitting include the need to assess the risks of CO_2 leakage and seismic activity associated with injection. Notably, despite more than 70 pending applications to the Environmental Protection Agency (EPA), no permits have been issued since 2020, highlighting the challenges and risk assessments needed for permitting.[3,5] Furthermore, there are extensive requirements for monitoring injection projects, which drives up costs as large areas need to be monitored, sometimes for decades.[3] Importantly, many regions do not have appropriate geology for CO_2 sequestration, which will pose additional challenges[6,7] to the development of the CCS industry in many nations.

The alternative to reservoir injection is storage in saline aquifers or CO_2 mineralization in geological sites of rocks like basalt, etc.[8,9] However, the area footprint of mineralization projects is much larger than injection projects, which increases costs.[3] Microbial CO_2 sequestration has low energy intensity and is environmentally friendly;[10] however, the efficiency of microbial CO_2 fixation is low. Other alternatives to sequestration include embedding CO_2 in concrete,[11] chemicals,[12] etc. While these are very promising, such approaches by themselves will not be sufficient to address gigascale sequestration

Received: May 7, 2024
Revised: May 23, 2024
Accepted: May 24, 2024

requirements. Overall, additional options for sequestration need to be urgently added to the basket of available solutions.

This study enables a disruptive approach to the synthesis of CO_2 hydrates for sequestration. CO_2 hydrates[13,14] are ice-like crystalline materials synthesized from CO_2 and water at medium pressures (~2.86 MPa) and low temperatures (<5 °C); these conditions are prevalent in large parts of the seabed worldwide. Structurally, CO_2 hydrates consist of a cage of water molecules that trap a CO_2 molecule. On average, 6 water molecules trap 1 molecule of CO_2. One kilogram of solid CO_2 hydrate can sequester up to 290 g of CO_2 (i.e., 150 L of CO_2 at 25 °C and 1 atm). Importantly, CO_2 hydrates are denser than seawater (density: 1040−1160 kg/m^3).[15]

Hydrate-based CO_2 sequestration in subsea porous media under marine sediments has been recently proposed.[6,16,17] Alternatively, hydrates could be stored on the seabed if they are encapsulated by appropriate sealing materials. Sealing is essential to prevent the dissociation of hydrates in seawater, as was seen in previous field tests.[18,19] Seabed sequestration will also need regulatory changes in view of the London Protocol.

Hydrates offer another important value proposition in CCS; this involves lowering the overall CCS costs by reducing the need for the purification of CO_2. The current practice of reservoir injection requires CO_2 purity levels >95%.[3] Purification of captured CO_2 is a major contributor to overall costs. In contrast, hydrates can be formed from flow streams with CO_2 purity levels of 40−60%, which significantly lowers the cost of purification, thereby increasing the overall economic viability of CCS.

A key technical challenge to any hydrate-based approach is the very slow formation of hydrates. Gas hydrates (CO_2, methane) can take hours to days[14,20,21] to nucleate in the absence of external promotion techniques. Chemical promotion and mechanical agitation are commonly used[14] to initiate nucleation. However, post nucleation, the growth rate is limited by multiple factors. Gas diffusion through the already-formed hydrate shell/layer slows down further growth.[22] Heat transfer considerations[23,24] also influence the growth rate since the heat released from hydrate formation needs to be removed. Solutions to enhance growth include the use of kinetic and thermodynamic promoters,[25,26] mechanical agitation,[27] electronucleation,[23] etc. However, using such approaches increases the complexity of operations; besides, the use of chemicals is undesirable.

Even with the use of the above techniques, hydrate formation remains slow. Table 1 summarizes the results of nine experimental studies on CO_2 hydrates; these studies reported the highest CO_2 gas consumption rates across the literature. To compare hydrate formation rates across different studies, we have devised a metric of gas consumption rate per unit volume of reactor per unit excess pressure (from the equilibrium pressure). This is the normalized rate (unit: g h^{-1} L^{-1} MPa^{-1}) at which CO_2 can be sequestered and is termed as sequestration rate ($\dot{m}_S$) in this study. This metric is analogous to the metric of the overall mass transfer coefficient, which is commonly used to compare the carbon capture performance of various systems. Importantly, this accounts for the varied operating conditions in various studies. The highest sequestration rates in the literature were observed for sequestration using packing columns due to their high area-to-volume ratio. The highest rates reported are 209.7 and 200.6 g h^{-1} L^{-1} MPa^{-1} for a horizontal packed bed with copper foam and SSP-2 metallic packing, with the use of 1 wt % SDS solution, respectively.[30−32] It is important to note that most other studies report much lower numbers.

Table 1. Compilation of Key Studies Reporting CO_2 Hydrate Formation in Flow-Based Reactors

refs	pressure, temperature	experimental setup	gas mixture and promoter	gas consumption rate (m_{gcrS} in [g h^{-1}])	sequestration rate ($\dot{m}_S$ in [g h^{-1} L^{-1} Mpa^{-1}])	highlights
18,19	12 MPa, 3.3 °C	continuous jet coflow reactor	CO_2 (l) and water; no promoters	0.64	-	tubular paste-like hydrate plumes sink in the ocean. CO_2 dissociates.
28	3.5 MPa, 2.5 °C	water spray in reactor (173 mm dia, 568 mm height); 1.3 L	oscillating CO_2 supply; no promoters	28.6	12.0	larger nozzle atomizing angle increases hydrate formation
31,32	5 MPa; 0.9 °C	horizontal packed bed reactor with Cu foam; 1 L	CO_2/CH_4 mixtures; tryptophan, cyclopentane	231.7	209.7	high liquid−gas contact area and tryptophan is essential for rapid kinetics
30	3 MPa; 1.5 °C	SSP-2 metallic packing; 0.4 L reactor	pure CO_2; 1 wt % SDS	121.44	200.6	packing with high area/volume ratio improves kinetics
35	3.5 MPa, 4.1 °C	magnetic stirrer (300 rpm); 0.5 L reactor	pure CO_2; nanofluid with 0.4% graphite nanoparticles	7.2	9.6	graphite nanoparticles increase maximum CO_2 consumption by 12.8%
33	3.5 MPa; 1.5 °C	mechanical stirrer (600 rpm); 0.3 L reactor	pure CO_2; 5 wt % decylamine	16.62	27.5	decylamine aqueous solution shows best kinetic performance
29	2.5 MPa, 0.6 °C	mechanical stirrer with CO_2 recirculation; 1.9 L	CO_2/N_2 mixtures; THF as promoter	0.67	0.3	mechanical agitation consumes significant power
34	7.5 MPa; 0.6 °C	magnetic stirrer; 0.32 L	CO_2/N_2, CO_2/H_2; no promoters	18.56	35.2	CO_2 separation from CO_2/N_2 and CO_2/H_2 mixtures deemed viable
36,37	3 MPa; 1 °C	bubble column reactor (0.1 × .1 × 4 m^3); 40 L	CO_2/H_2, pure CO_2; TBAB as promoter	24	0.82	gas bubbles form hydrate shells that coalesce to form hydrate foam. The optimal bubble size is 50 μm
this study	3.55 and 2.85 MPa; 2.6 ± 0.8 °C	bubble column reactor (63.5 mm dia, 152 mm depth); 0.65 L	pure CO_2; no chemical promoter used, Mg used	1601.6	1276.5	increased pressure, flow rates and amount of Mg increase sequestration rate

https://doi.org/10.1021/acssuschemeng.4c03809
ACS Sustainable Chem. Eng. XXXX, XXX, XXX−XXX

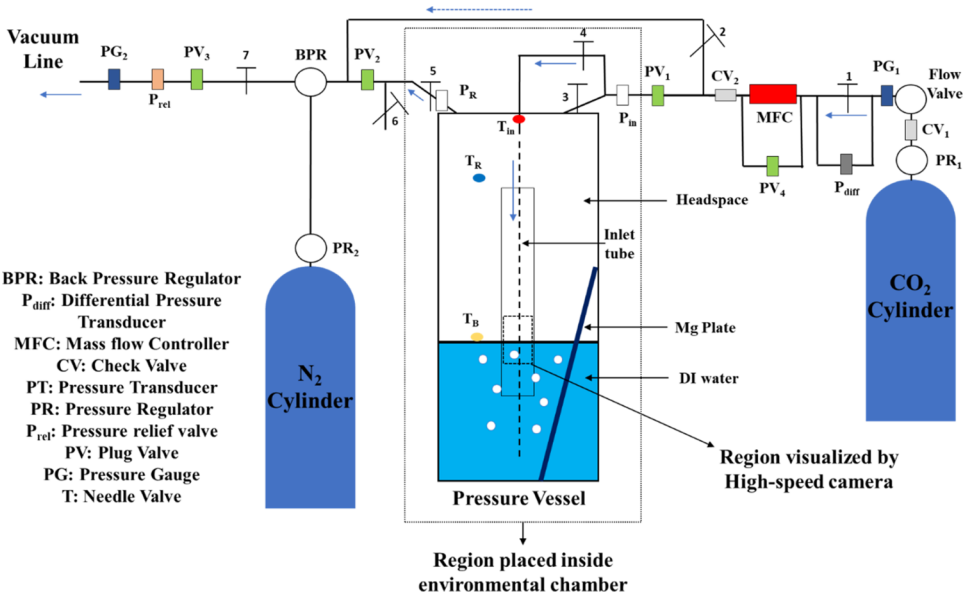

Figure 1. Schematic of the experimental setup used in the study.

Mechanical agitation using magnetic or mechanical stirring has been used to enhance hydrate formation;[29,33,34] however, this involves significant power consumption.[29] Nanofluids with graphite nanoparticles were shown to increase formation kinetics and maximum CO_2 uptake.[35] The influence of chemicals like decylamine, amylamine, and methylamine on hydrate formation and dissociation kinetics has been studied; 5 wt % decylamine showed the best results.[33] In a field test, a continuous jet coflow reactor was used to create and deploy hydrate plumes into the ocean at 1200 m depth (~12 MPa).[18,19] In another study, a water-spray apparatus with an oscillating CO_2 supply was used to enhance hydrate growth.[28] In a larger scale study, a 40 L bubble column reactor was used to study CO_2 hydrate formation.[36,37] Shells of hydrates formed on the bubbles and then coalesced to eventually form hydrate foam; however, the sequestration rate was significantly lower than that observed with metallic packing.

It is noted that most such studies require the use of chemical promoters like SDS, tryptophan, THF, TBAB, and cyclopentane to enhance hydrate formation kinetics. While some of these promoters are biofriendly (like tryptophan), the use of chemical promoters is undesirable as they increase cost, increase operational complexity, reduce CO_2 removal from a life-cycle standpoint, reduce overall sustainability, and can even be carcinogenic.[38] This highlights the importance of developing sustainable, biofriendly approaches for rapid hydrate formation.

Presently, we report a new advancement that enables sequestration rates of up to 1.28 kg h^{-1} L^{-1} MPa^{-1}; this is >6 times higher than the state-of-art. This finding is even more significant since we do not use any conventional chemical promoter, mechanical agitation, packing columns, or electric fields. Our advancement leverages and couples two distinct and recent discoveries from our group. The first is our discovery of magnesium as a promoter of CO_2 hydrate nucleation.[14] In this study, we further discover that magnesium is critical to rapid formation (beyond nucleation), as well. Second, we employ a novel approach to enhance hydrate growth; this involves high flow rate sparging use of CO_2 in an open reactor. An open reactor allows heat from hydrate formation to be easily dissipated away by the continuous influx of incoming gas. Additionally, the constant inflow and outflow of gas bubbles results in continuous renewal of the gas−water−hydrate interface, which enhances the growth significantly. Overall, high flow rates help increase the rate of hydrate formation via enhanced mass and heat diffusion and disruption of existing hydrate shells. Our recent simulations[39] to predict hydrate formation in bubble column reactors also showed that the hydrate formation rate will increase with the CO_2 flow rate (details in the Supporting Information); we benefit from this insight in the present study. In addition to measuring the growth rate, we also estimate the conversion fraction of CO_2 into hydrates, which is an important parameter that determines the need for recirculation. Furthermore, our novel analytical approach evaluates the composition of the hydrate formed, which can be used to distinguish between gas consumed by water as hydrates or dissolved gas and unreacted CO_2 gas trapped inside hydrate shells. Overall, this study opens up a novel technological option targeted at sustainability and environmental protection. Additionally, this study also opens up new avenues in other sustainability-related areas, like desalination via hydrate formation and hydrogen storage via hydrates.

EXPERIMENTAL METHODS

CO_2 gas (99.9% pure) was bubbled into a stainless-steel reactor (inner diameter: 6.35 cm; depth: 15 cm) housed inside an environmental chamber for temperature control. The reactor contained 200 mL of deionized (DI) water with a conductivity of ≤1.0 μMhos and a magnesium alloy (AZ31) plate (10.1 cm × 1.25 cm). A detailed schematic of the entire setup is shown in Figure 1.

Experiments were conducted at a reactor temperature $T_R = 2.6 \pm 0.8$ °C. The reactor was purged of air by bubbling CO_2 at 0.8 slpm (at atmospheric pressure) for 5 min. Next, the reactor was pressurized at 60 psi/min until the reactor pressure (P_R) reached the pressure set point (P_{set}). Hydrates started forming toward the end of the pressurization stage itself, and this is consistent with the ultrafast nucleation (due to magnesium) reported in our previous study.[14] Therefore, in this study, the formation time (t_f) was estimated from the instant when reactor pressure and temperature conditions entered the hydrate stability zone. The pressurization stage was followed by a constant flow rate at constant pressure ($P_R = P_{set} = 2.86$ MPa (400 psig) or 3.55 MPa (500

https://doi.org/10.1021/acssuschemeng.4c03809
ACS Sustainable Chem. Eng. XXXX, XXX, XXX−XXX

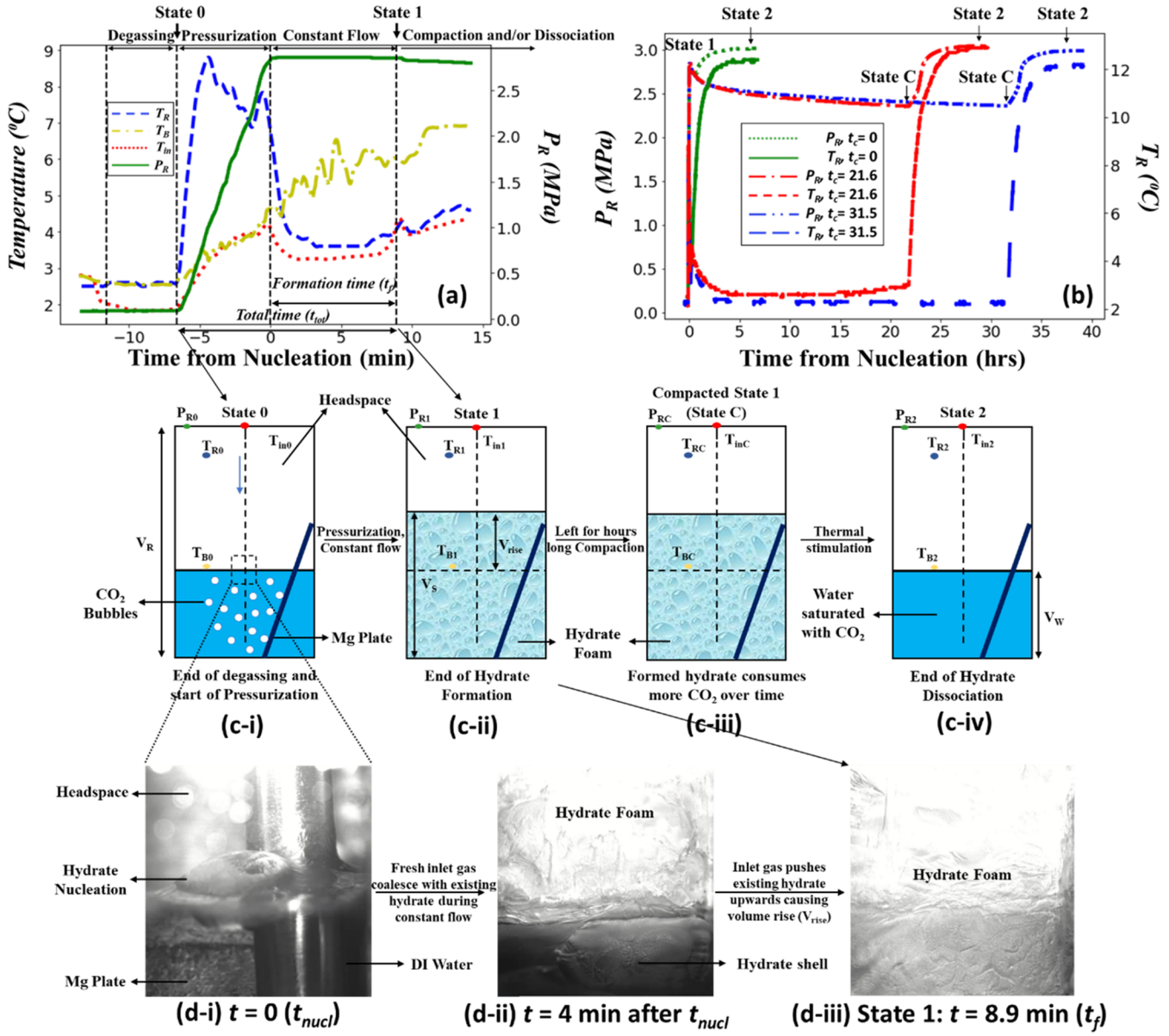

Figure 2. Overview of experimental procedure and results. (a) Time variation of reactor pressure (P_R), reactor temperature (T_R), inlet gas temperature (T_{in}), and water temperature (T_B) during the experiment. (b) Time variation of reactor pressure (P_R) and reactor temperature (T_R) for two compaction experiments and one no-compaction experiment. (c) Schematic depiction of hydrate formation in the reactor at (i) State 0: beginning of pressurization. (ii) State 1: end of hydrate formation (after constant gas flow); (iii) State C (compacted state): achieved after closing the inlet and outlet of the reactor and letting hydrates compact over many hours; and (iv) State 2: end of hydrate dissociation. (d) Images of the dashed region marked in c-i at (i) onset of nucleation, (ii) 4 min after nucleation, and (iii) end of constant flow (State 1: $t = t_f$ = 8.9 min).

psig)), maintained using a back-pressure regulator and a mass flow controller (FMA 5523A).

During the constant flow stage, bubbles rise and stick to existing hydrates. Subsequently, a hydrate shell is formed with gas trapped inside, as also observed in related studies.[36,37] Incoming gas forces these shells to coalesce, building up a mixture of hydrate crystals, trapped CO_2 gas inside and around the hydrate shells, and unreacted water with dissolved CO_2. This mixture is termed as hydrate foam in this study as it is a porous hydrate structure with unreacted water and trapped gas inside it. The volume of this foam is greater than the initial volume of water (Figure 2c); this volume rise can be measured. Temperatures are measured at three locations: gas at the inlet of the reactor (T_{in}), at the interface of water and gas (T_B), and gas (T_R) in the headspace of the reactor (Figure 2c). The inlet and outlet of the reactor are closed at the end of the constant flow (State 1), wherein T_{B1} is the temperature of the hydrate foam, T_{R1} is the gas temperature in the headspace, and P_{R1} is the reactor pressure. The foam temperature helps analytically evaluate the foam composition, as discussed in detail in the Supporting Information.

Variations of the temperature and pressure during degassing, pressurization, constant flow, and compaction are provided in Figure 2a. It is observed that the temperatures within the reactor vary significantly during the course of the experiment, highlighting the importance of multiple temperature sensors within the reactor. The gas headspace temperature (T_R) spikes initially at the start of pressurization due to the sudden change in the working pressure. Once the operating pressure is reached, the headspace temperature is observed to stabilize at a much lower value. Similarly, the interface temperature or bulk temperature (T_B) also increases during pressurization but at a much slower rate. This is because water has a higher thermal inertia than the gas headspace. Unlike the gas headspace temperature, the interface temperature continues to increase even after the pressure stabilizes. This is because hydrate nucleation and subsequent growth are observed

https://doi.org/10.1021/acssuschemeng.4c03809
ACS Sustainable Chem. Eng. XXXX, XXX, XXX−XXX

Table 2. Compilation of All Hydrate Formation Experiments in This Study[a]

P_{set} [MPa]	subcooling [°C]	water type and other special conditions	total flow time t_{tot} [min]	flow rate of gas $\dot{m}_{in}$ [slpm]	CO_2 in foam $m_{C,S}$ [g]	sequestration rate $\dot{m}_S$ [g h^{-1} L^{-1} MPa^{-1}]	volume fraction of foam(V_S/V_R)	% conversion of CO_2 to foam	density of foam relative to water (ρ_S/ρ_w)
3.55 ± 0.1	6.0 ± 0.1	DI water	15.25 (t_f = 1.25)	10.3 ± 2.8	33.8 ± 0.8	1276.5 ± 32.9	0.61 ± 0.01	-	0.59 ± 0.01
3.55 ± 0.1	6.6 ± 0.1	DI water	16.75 (t_f = 1.55)	10.8 ± 0.3	32.9 ± 0.7	977.7 ± 42.3	0.57 ± 0.01	-	0.60 ± 0.01
3.55 ± 0.1	5.3 ± 0.1	saltwater	17 (t_f = 2.5)	10.7 ± 0.4	36.6 ± 0.8	871.5 ± 4.8	0.61 ± 0.01	69.9 ± 2.5	0.58 ± 0.01
3.55 ± 0.1	5.1 ± 0.1	saltwater	17 (t_f = 2.28)	10.6 ± 0.3	35.3 ± 0.7	973.6 ± 12.1	0.59 ± 0.01	74.1 ± 2.1	0.60 ± 0.01
3.55 ± 0.1	5.2 ± 0.1	saltwater	16 (t_f = 3)	9.7 ± 0.4	34.4 ± 0.7	733.3 ± 13.8	0.60 ± 0.01	59.9 ± 2.6	0.58 ± 0.01
2.86 ± 0.1	4.0 ± 0.1	DI water	15.5 (t_f = 8.9)	10.8 ± 0.8	29.5 ± 0.7	259.3 ± 6.0	0.62 ± 0.01	15.6 ± 0.9	0.56 ± 0.01
2.86 ± 0.1	3.9 ± 0.1	DI water	14 (t_f = 7.3)	10.7 ± 0.6	24.4 ± 0.6	275.3 ± 6.5	0.54 ± 0.01	16.0 ± 0.7	0.63 ± 0.01
2.86 ± 0.1	4.4 ± 0.1	DI water	14 (t_f = 7.3)	10.8 ± 0.3	24.1 ± 0.6	252.9 ± 6.0	0.55 ± 0.01	15.7 ± 0.5	0.61 ± 0.01
2.86 ± 0.1	4.1 ± 0.1	DI water	14 (t_f = 7.3)	10.7 ± 0.6	24.9 ± 0.6	268.1 ± 6.3	0.56 ± 0.01	16.2 ± 0.8	0.61 ± 0.01
2.86 ± 0.1	4.2 ± 0.1	DI water	13 (t_f = 6.5)	10.7 ± 0.5	21.9 ± 0.5	262.0 ± 6.3	0.50 ± 0.01	16.1 ± 0.7	0.68 ± 0.02
2.86 ± 0.1	3.6 ± 0.1	DI water	12 (t_f = 5.2)	10.8 ± 0.5	17.4 ± 0.4	283.6 ± 7.2	0.41 ± 0.01	15.7 ± 0.7	0.80 ± 0.02
2.86 ± 0.1	4.5 ± 0.1	DI water	15.5 (t_f = 9.2)	8.1 ± 0.6	27.0 ± 0.6	215.4 ± 5.0	0.58 ± 0.01	18.4 ± 1.0	0.59 ± 0.01
2.86 ± 0.1	3.3 ± 0.1	DI water	15.5 (t_f = 8.5)	4.5 ± 0.6	15.8 ± 0.4	170.9 ± 4.4	0.39 ± 0.01	21.3 ± 2.1	0.85 ± 0.02
2.86 ± 0.1	3.3 ± 0.1	DI water	15.5 (t_f = 8.5)	3.5 ± 1.4	15.1 ± 0.4	159.8 ± 4.2	0.39 ± 0.01	25.9 ± 8.7	0.84 ± 0.02
2.86 ± 0.1	4.0 ± 0.1	DI water used; 6× Mg	14 (t_f = 7.2)	10.7 ± 0.5	29.7 ± 0.7	326.0 ± 7.5	0.6 ± 0.01	19.6 ± 0.9	0.58 ± 0.01
2.86 ± 0.1	1.9 ± 0.1	saltwater	160 (t_f = 152.8)	10.6 ± 0.4	23.0 ± 0.6	13.9 ± 0.3	0.36 ± 0.01	0.7 ± 0.03	0.95 ± 0.02
2.86 ± 0.1	4.5 ± 0.1	tapwater	14 (t_f = 7.4)	10.6 ± 0.6	27.9 ± 0.6	278.6 ± 6.5	0.60 ± 0.01	18.1 ± 0.9	0.58 ± 0.01
2.86 ± 0.1	4.4 ± 0.1	DI water; no Mg used	>30	10.8 ± 0.8	no hydrate nucleation observed even after 30 min.				
3.55 ± 0.1	5.2 ± 0.1	saltwater; no Mg used	>30	10.6 ± 0.8	no hydrate nucleation observed even after 30 min.				

[a]The temperature of the environmental chamber before degassing was 2.3 ± 1.1 °C.

at the interface upon reaching operating pressure. The exothermic nature of hydrate formation causes the interface temperature to rise during the constant flow stage. The temperature of the inlet gas (T_{in}) follows a similar trend as the gas headspace temperature since it also measures the temperature of a gaseous system and is not in direct contact with hydrate growth. The sensitivity to pressure change at this temperature is low because it is embedded within a 1/4 in. OD stainless-steel tube. In two experiments (Table 2), the reactor was left closed for a few hours to compact the hydrate foam. Hydrates were observed to form along the walls of the reactor during this stage. The corresponding volume increase was neglected, and the volume of hydrate foam in the compacted stage was considered to be the same prior to compaction. Compaction resulted in a significant decrease in pressure as the gas converted to hydrate and the temperature of the reactor stabilized. Compaction times (t_c) of 21.6 and 31.5 h were presently studied.

To end the experiment, the temperature was increased to 12.1 ± 0.2 °C, which resulted in a dissociation-induced pressure rise. The reactor was left for 8+ h to reach thermodynamic equilibrium. At the end of this step (state 2), it can be assumed that the water is saturated with CO_2 and is in thermal and mass equilibrium with the gas above. The reactor was then depressurized to end the experiment. Water volume was confirmed to be unchanged at the end of the experiment.

Video 1 (Supporting Information) shows various stages (pressurization, nucleation, and constant flow stages) associated with hydrate formation in the present experiments. Nucleation clearly occurs at the gas−water interface and is followed by the growth of individual hydrate shells/films, which are continuously compacted by incoming gas bubbles.

Analysis Framework. This subsection describes a novel analytical framework to estimate the formation rate and conversion fraction in our experiments. It is based on using measurements of pressure, temperature, and volume change (due to hydrate foam formation) to estimate the amount of CO_2 and its distribution in the reactor at State 1, which corresponds to the end of the constant flow stage (hydrate foam formation stage). In state 1, CO_2 exists in one of these forms: (i) as gas in the headspace ($m_{C,ga}$), (ii) absorbed by water as hydrates or dissolved gas ($m_{C,hw}$), or (iii) as unreacted gas trapped in the foam ($m_{C,gt}$). Importantly, our framework can quantify this distribution of CO_2 at the end of the hydrate formation stage. Our analysis approach is briefly described ahead with more details (and results on the composition of foam) along with a detailed nomenclature provided in the Supporting Information.

The volume rise of the hydrate foam column causes a change in the volume of headspace from state 1 to state 2. Reactor pressure, temperature, and volume of headspace at states 1 and 2 can be used to obtain the mass of CO_2 in the headspace at states 1 and 2 ($m_{c,ga1}$ and $m_{c,ga2}$). Henry's law[40] can be used to estimate the amount of CO_2 dissolved in water at state 2 ($m_{c,w2}$), assuming complete solubility. Summing the two masses of CO_2 in state 2 gives the total mass of CO_2 in the reactor ($m_{c,T}$), noting that no hydrates are present at state 2. The pressure driving force is obtained from the reactor pressure (P_R) during hydrate formation (P_{set}) and equilibrium pressure corresponding to the temperature before pressurization ($P_{eq}(@T_{R0})$). Similarly, the temperature driving force (or subcooling) is the difference between the temperature before pressurization (T_{R0}) and the equilibrium temperature at operating pressure ($T_{eq}(@P_{set})$). A detailed discussion on the evaluation of pressure and temperature subcooling for saltwater and DI water mixtures is provided in the Supporting Information. The rate at which the mass of CO_2 is consumed as hydrate foam ($\dot{m}_{gcr}$) can be obtained from eq 1 by using the formation time (t_f). This rate can also be written in the form of a kinetics growth equation using the pressure driving force ($P_R - P_{eq}$) and the kinetic rate constant (K). The sequestration rate ($\dot{m}_S$) is obtained by normalizing the kinetic rate constant over reactor volume, as shown in eq 3.

$$\dot{m}_{gcr} = \frac{m_{C,ga2} + m_{C,w2} - m_{C,ga1}}{t_f} \quad (1)$$

$$\dot{m}_{gcr} = K(P_R - P_{eq}(@T_{R0})) \quad (2)$$

https://doi.org/10.1021/acssuschemeng.4c03809
ACS Sustainable Chem. Eng. XXXX, XXX, XXX−XXX

$$\dot{m}_S = \frac{K}{V_R} = \frac{m_{C,ga2} + m_{C,w2} - m_{C,ga1}}{t_f V_R (P_R - P_{eq}(@T_{R0}))} \quad (3)$$

The composition of foam is estimated by dividing the total volume of foam (V_S) into the volume fraction of unused water (Y_w), the volume fraction of hydrate (Y_h), and the volume fraction of trapped gas inside foam (Y_{gt}). The unknown volume fractions can be evaluated by equating the total mass of water ($m_{w,T}$) and total mass of the system (CO_2 + water, i.e., $m_{C,T} + m_{w,T}$) in states 1 and 2 (eqs 4 and 5). The total mass of water is split into mass of unused water (molecular weight M_w) and mass of water in the form of hydrate (molecular weight M_h) as depicted in eq 4. Depending on the cage occupancy and structure of the hydrate formed, the hydration number (η_h) can vary between 5.75 and 7. However, the key results were not sensitive to the hydration number. Therefore, as standard practice, a hydration number of 6 and hydrate density (ρ_h) of 1100 ± 60 kg/m^3 was used in this study.[6] The volume fractions, along with the density of water (ρ_w), hydrate (ρ_h), and trapped gas (ρ_{gt}, obtained from compressibility equation at temperature T_{B1}), can be used to evaluate the contribution of individual components of foam to the total mass of the system (CO_2 + water) in state 1. The sum of the mass of hydrate foam and the mass of CO_2 in the headspace ($m_{c,ga1}$) would be equal to the total mass in state 1 (eq 5). Once the volume fractions are evaluated, the mass distribution of CO_2 and water in various phases can be obtained.

$$m_{w,T} = \rho_w Y_w V_S + \rho_h Y_h V_S M_w \eta_h / M_h \quad (4)$$

$$m_{C,T} + m_{w,T} = m_{C,ga1} + Y_w V_S \rho_w + Y_h V_S \rho_h + Y_{gt} V_S \rho_{gt} \quad (5)$$

The conversion fraction was evaluated as the ratio of the net amount of CO_2 sequestered in the hydrate foam and the mass of CO_2 entering the reactor during the formation time of t_f (eq 6).

$$\%\ \text{conversion} = \frac{m_{C,ga2} + m_{C,w2} - m_{C,ga1}}{\dot{m}_{in} t_f} \times 100 \quad (6)$$

RESULTS AND DISCUSSION

Hydrate formation will increase with lower temperatures and higher pressures. Constraints on the P-T window in our flow reactor-based experiments arise from the need to prevent ice formation (which will unnecessarily consume water) or liquid CO_2 formation (which will slow hydrate formation). Accordingly, our most aggressive thermodynamic conditions for hydrate formation in this study were 3.55 MPa (500 psig) and 1.6 °C. However, for these conditions, the presence of magnesium immersed in water caused hydrate formation to begin during the pressurization stage itself (at around 2.86 MPa (400 psig)). While this is a very significant and beneficial finding, this preemptive nucleation significantly hindered the conduct of experiments required for a detailed parametric assessment at 3.55 MPa. Detailed studies on the influence of various parameters were therefore conducted at 2.86 MPa (400 psig) and are discussed in a later section.

The experimental procedure to conduct experiments was modified slightly to enable the conduct of a few experiments at 3.55 MPa (500 psig). A magnesium plate (1 cm × 1 cm) was suspended in the headspace using magnets across the glass window in the reactor. Once the set pressure was reached, the system was allowed to stabilize its temperature for another ∼7−8 min before magnesium-water contact was initiated by dropping the magnesium plate using a magnet-based release arrangement. While this magnet-based plate worked for most cases, it was observed that oftentimes hydrates started forming before the plate release (during pressurization or stabilization stages), further adding to the difficulty in conducting a detailed parametric variation study. We report five successful experiments at 3.55 MPa (500 psig): 2 experiments with DI water and 3 experiments with saltwater (sodium chloride concentration of 3.5 wt %) to mimic seawater. For the DI water experiments, hydrates nucleated immediately after dropping the magnesium plate (Video 4 in the Supporting Information). For two out of three experiments with saltwater, nucleation occurred 30 and 43 s from the time the magnesium plate was released in water. For the third experiment with saltwater, nucleation occurred during the stabilization stage, and the plate was dropped 10 s after nucleation.

In the best result with DI water (3.55 MPa (500 psig)), 33.8 g of CO_2 was consumed in the hydrate foam within 75 s. The corresponding gas sequestration rate was 1276.5 g h^{-1} L^{-1} MPa^{-1} (Table 2), which is more than 6 times greater than the highest sequestration rate of CO_2 hydrates reported in the literature (i.e., 209.7 g h^{-1} L^{-1} MPa^{-1}).[30] Hydrate formation with DI water at 3.55 MPa (500 psig) was studied for a low formation time of 75 and 90 s because the hydrate foam went above the glass window on the reactor in this time, and continuous flow was then stopped to accurately measure the volume rise due to hydrate formation (V_S/V_R). While it is expected that hydrate formation rates will be high initially and then slow down, such a relation is not as prominent in an open system as also shown in a subsequent section (Figure 5). Furthermore, the highest hydrate formation rate reported in the literature,[30] to which our results are compared, also corresponds to the highest instantaneous rate in that study.

In the best result with saltwater, 35.3 g of CO_2 was consumed in the hydrate foam within 137 s with a corresponding sequestration rate of 973.6 g h^{-1} L^{-1} MPa^{-1} (Table 2), which is 4.6× the highest reported in the literature for DI water. These numbers are in line with the understanding that the presence of salt in water slows hydrate formation.[41] The fact that we still get significant enhancement with saltwater use is very promising, as costs associated with water desalination can be avoided by using seawater.

This significant enhancement is the result of magnesium-based promotion coupled with the benefits of constant gas flow in an open system and a high water−gas-hydrate interfacial area for a given reactor size. Our previous study[14] examined only the nucleation-promotion aspect of magnesium and the underlying mechanisms behind it; this study quantifies the benefits of magnesium for overall hydrate formation. We reiterate that magnesium is a key enabler of this concept, as there was no hydrate formation observed for over 30 min in the absence of magnesium (Table 2). Notably, the hydrate formation rate with DI water at 3.55 MPa (500 psig) was 6 times higher than similar experiments conducted at 2.86 MPa (400 psig) (Table 2). Further experiments and a parametric study were conducted at 2.86 MPa (400 psig) due to significant ease in experimentation, as discussed earlier.

Influence of Inlet Gas Flow Rate on Hydrate Formation. Experiments were conducted for total flow time (t_{tot}) (pressurization + constant flow) of 14 min at 2.86 MPa (400 psig) and 2.6 ± 0.8 °C. The inlet gas flow rate ($\dot{m}_{in}$) was varied in the range of 3.5−10.8 slpm. A higher flow rate is expected to increase hydrate formation due to enhanced mass transfer, breakage of hydrate shells, and better heat removal.[39] Indeed, Figure 3 shows that sequestration rate ($\dot{m}_S$) increases with the flow rate, thus sequestering more CO_2 per given mass of water ($m_{C,S}/m_{w,T}$ is shown on the secondary y-axis). It is reasonable to assume that large quantities of trapped gas will convert to hydrates as the hydrate foam is transported (to the

https://doi.org/10.1021/acssuschemeng.4c03809
ACS Sustainable Chem. Eng. XXXX, XXX, XXX−XXX

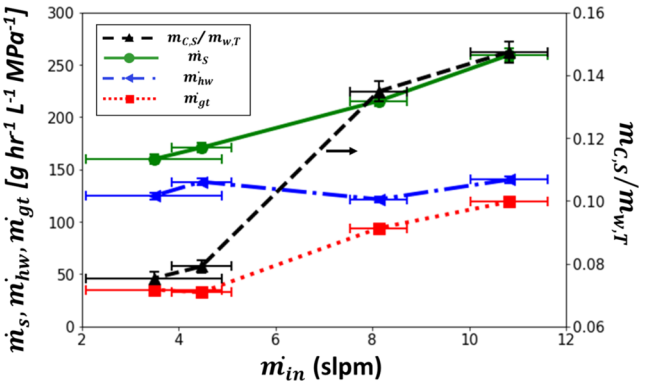

Figure 3. Influence of inlet gas flow rate ($\dot{m}_{in}$) on CO_2 sequestration rate ($\dot{m}_S$), gas consumption rate associated with hydrate formation ($\dot{m}_{hw}$), and trapped gas consumption rate ($\dot{m}_{gt}$). The ratio of the mass of CO_2 sequestered in hydrate foam to the mass of water ($m_{C,S}/m_{w,T}$) is shown on the secondary *y*-axis.

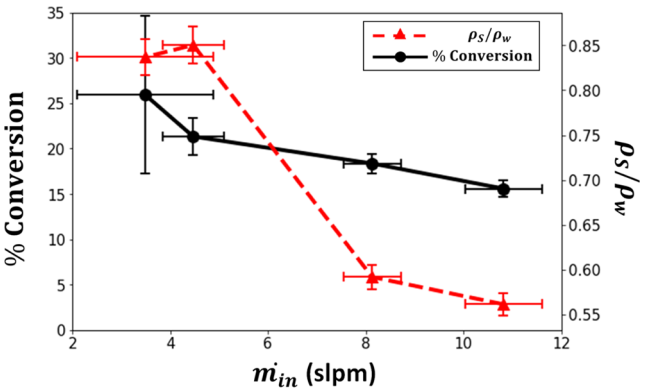

Figure 4. Influence of the inlet gas flow rate ($\dot{m}_{in}$) on conversion fraction. The density of hydrate foam relative to water (ρ_S/ρ_w) is shown on the secondary *y*-axis.

sequestration site) over significant distances. This implies that higher $m_{C,S}/m_{w,T}$ would generate a higher wt % foam for sequestration, which indicates better water utilization. Analysis of the components of the sequestered gas leads to interesting insights, noting that the sequestrated CO_2 includes unreacted trapped gas ($\dot{m}_{gt}$) and the gas converted to hydrate ($\dot{m}_{hw}$). It is seen that gas conversion to hydrates ($\dot{m}_{hw}$) stays roughly constant for the >3× increase in the gas flow rate. Visual examination (Video 2 in the Supporting Information) reveals that at high flow rates, fresh hydrate shells stick and coalesce with the hydrate mass due to the upward momentum of the incoming gas. This increases the volume fraction of the foam (V_S/V_R), accompanied by an increase in the amount of unreacted trapped gas. The overall increase in the sequestration rate as hydrate foam is primarily due to this increase in trapped unreacted gas ($\dot{m}_{gt}$). This suggests that mechanisms that enhance mass transfer will further increase hydrate formation. The addition of mechanical agitation or the use of sprays will facilitate the breakup of hydrate shells and enhance hydrate formation, as will the mixing during hydrate foam transportation.

The energy required to produce a hydrate foam and the quality of the foam also changes with the increasing inlet gas flow rate. The energy requirement depends on the power to pump gas and the need for recirculation, which in turn depends on the conversion fraction which decreases with increasing flow (Figure 4). The conversion fraction decreases at a slow rate from 25.9 to 15.6% for a 308% increase in the gas flow rate. In comparison, the sequestration rate increases by 1.62 times for this increase in the flow rate. This is an important finding that suggests that high flow rates will increase the sequestration rate without drastically changing recirculation requirements. The reported conversion fractions in this study are low compared to the existing literature.[36] This is because the goal here is hydrate-based sequestration and not gas separation. The pressure rise needed for the recirculation of gas is significantly lower than the pressure rise for fresh gas to be brought to the operating pressure. This suggests that a high conversion fraction is not an essential requirement for ultrafast hydrate formation since the unreacted gas can be recirculated. A low conversion factor would also imply low water consumption for hydrate formation (~20%, as shown in the Supporting Information), but the excess water can also be easily recirculated after the hydrate foam is compacted in a separate reactor before eventual sequestration.

The quality of the foam produced also changes significantly with the inlet gas flow rate. This foam includes hydrate crystals, unreacted trapped gas, and unreacted water. The increase in the fraction of unreacted gas inside the foam changes the quality of the foam, making it less dense (Figure 4). While unreacted trapped gas could appear problematic, it must be realized that a lot of this trapped gas will convert to hydrates while the foam is being transported for sequestration. Overall, Figures 3 and 4 highlight the benefits of high flow rate sparging of CO_2 for rapid foam formation for sequestration.

Influence of Formation Time on Hydrate Formation. Experiments were conducted to study the influence of formation time on the gas consumption rate: total flow time (t_{tot}) was varied from 12−15.5 min, with the reactor at 2.86 MPa (400 psig) and 2.5 ± 0.5 °C, and a flow rate of 11 ± 1 slpm. Figure 5

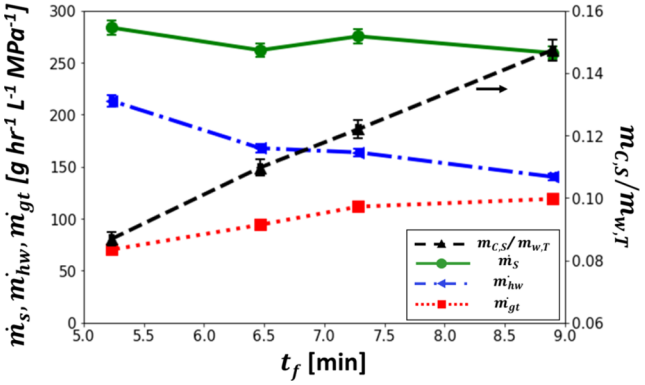

Figure 5. Influence of formation time (t_f) on the sequestration rate ($\dot{m}_S$), gas consumption rate associated with hydrate formation ($\dot{m}_{hw}$), and trapped gas consumption rate ($\dot{m}_{gt}$). The ratio of the mass of CO_2 sequestered in foam to the mass of water used ($m_{C,S}/m_{w,T}$) is shown on the secondary *y*-axis.

shows that the total mass of CO_2 sequestered as hydrate foam per unit mass of water ($m_{C,S}/m_{w,T}$) increases linearly with the formation time (t_f), which is critical from a scalability perspective. The sequestration rate is constant (266 ± 12 g h^{-1} L^{-1} MPa^{-1}) over this time range of time. This finding is significant as more gas can be sequestered for the same amount of water by running the reactor longer before the hydrate foam is extracted.

It is noted that although the sequestration rate is constant over time, the foam composition changes significantly (Figure 5). As

https://doi.org/10.1021/acssuschemeng.4c03809
ACS Sustainable Chem. Eng. XXXX, XXX, XXX−XXX

fresh gas forms hydrate shells (which attach to the existing hydrate mass and eventually coalesce), the amount of CO_2 as a hydrate and as gas trapped in the foam both increases, along with an increase in foam volume (V_S/V_R). However, the gas consumption rate of CO_2 in water (dissolved or as a hydrate crystal, i.e., m_{hw}) decreases with time by ∼35%, while the trapped, unreacted gas inside foam ($\dot{m}_{gt}$) increases with time by ∼70%. This is expected since hydrate formation is exothermic, which impedes further growth. Furthermore, from a mass transfer perspective, since a new hydrate comes in as a shell with unreacted CO_2 gas trapped inside it, a lesser water−gas contact area is available for further hydrate formation (since most of the unreacted trapped CO_2 gas in the foam is inside hydrate shells without water). Breaking up this foam will help further hydrate formation. Additional details on the distribution of mass fraction and volume fraction of CO_2 gas, liquid water, and CO_2 hydrate inside the reactor are provided in the Supporting Information.

Hydrate Formation From Impure Water. Additional experiments conducted in this study are summarized in Table 2. Experiments were conducted with saltwater (sodium chloride concentration of 3.5 wt % to mimic seawater) at 2.86 (400 psig) and 3.55 MPa (500 psig). At 2.86 MPa and 2.5 ± 0.5 °C, the amount of gas consumed by saltwater was 23 g in 160 min; this is in contrast to 24.5 g of gas consumption in 14 min for DI water. This corresponds to the sequestration rate using saltwater being 18 times slower than that with DI water. This is expected as salt ions slow down hydrate formation.[41] Visually, there is a noticeable difference in hydrate formation from saltwater versus DI water at 2.86 MPa. Unlike the coalescence of hydrate shells seen with DI water, experiments with saltwater showed a gradual increase in opacity of the saltwater solution over the gas flow time of 160 min (Video 3 in the Supporting Information). This causes a low rise in the hydrate foam volume (V_S/V_R) when compared to the DI water experiments. The density of the hydrate foam formed in 160 min from saltwater is 950 kg/m^3, which is 56% higher than that of the foam from deionized water under the same conditions in 14 min. This is an important finding implying that denser hydrate foams (which require lesser compaction) can be formed with saltwater at lower pressures; however, the corresponding sequestration rate will be significantly lower. It is to be noted that there was almost no foam formation observed for saltwater in 14 min (at 2.86 MPa), whereas significant formation occurred in 14 min with deionized water.

In contrast, hydrate formation rates were comparable for saltwater and DI water at 3.55 MPa. For the three experiments conducted with saltwater at 3.55 MPa, the average sequestration rate was 859.5 ± 111.4 g h^{-1} L^{-1} MPa^{-1}, which is ∼62 times higher than that at 2.86 MPa. This discrepancy in formation with saltwater between 2.86 and 3.55 MPa was attributed to the low subcooling (or lower pressure driving force) provided to the system at 2.86 MPa (Table 2). For the 3.55 MPa experiments with saltwater, the subcooling was 5.2 °C. This is >2.5× times higher than the subcooling of 1.9 °C at 2.86 MPa. It is noted that the respective equilibrium curves for hydrate formation with saltwater and DI water were used to obtain subcooling of the system, as reported in Table 2 (details in the Supporting Information). Importantly, an experiment was conducted with tapwater to study the utility of this concept for nonpure water streams. At 2.86 MPa (400 psig) and 2.3 ± 0.3 °C, a total flow time of 14 min, and an inlet gas flow rate of 10.7 ± 0.4 slpm, a total of 27.9 g of CO_2 was sequestered using tapwater in comparison to 24.9 g for DI water. The corresponding sequestration rates for tapwater and DI water were 278.6 ± 6.5 and 259.3 ± 6 g h^{-1} L^{-1} MPa^{-1}, respectively, showing that similar sequestration rates can be achieved with tapwater and DI water. Taken together, these findings imply that while seawater-based hydrate formation will be challenging (even with the significant benefits of magnesium), the success of this approach does not require ultrapure water, which vastly simplifies operations and improves techno-economics.

Influence of Quantity of Magnesium on Hydrate Formation. Magnesium is a key enabler of our approach; accordingly, a separate experiment was conducted to quantify the influence of the quantity of magnesium on gas consumption. This involved the use of 2 magnesium plates, with each plate being 3 times the size of plates used in previous experiments. The gas consumption rate was found to increase (Table 2) from 275.3 to 326 g h^{-1} L^{-1} MPa^{-1} (18% increase) for the same conditions of 2.86 MPa (400 psig), 2.6 °C, a flow rate of 11 ± 1 slpm, and a total flow time of 14 min. This suggests that while more magnesium contact helps, the gains do not scale linearly.

It is noted that very little magnesium is consumed via our approach; this has also been discussed in our previous study.[14] Although a new magnesium plate was used for each experiment, reusing magnesium plates continued to result in vigorous hydrate formation. The structural integrity of the plate was observed to significantly change only after reusing the plate more than 4 times. Importantly, magnesium was in contact with water for 10+ h in every experiment, although its useful role was limited to the first few minutes only. This clearly suggests that very small quantities of magnesium are consumed during hydrate formation; this is in stark contrast to the relatively large quantities of chemical promoters used. For example, a 500 ppm concentration of SDS is commonly used for hydrate promotion.[38] The cost per gram of Mg alloy plate used in this study is $6/g, while the cost per gram of SDS is $0.6/g. Although the price per gram for Mg is higher, the consumption of Mg is negligible, while all of the SDS will be consumed. Considering the negligible consumption of Mg, the cost for using Mg is much lower than those of other promoters. Furthermore, there are significant additional costs associated with handling and disposal of chemicals, as there are environmental issues associated with chemical use. All of this highlights the importance of magnesium for hydrate promotion from an economic and sustainability perspective.

This study did not analyze the chemistry underlying magnesium-based growth promotion, noting that nucleation-promotion mechanisms were discussed in our previous study.[14] Mechanisms responsible for promotion[14] include higher water−hydrate−gas contact area (more nucleation sites), the reaction of oxide layer on magnesium with carbonated water, and the likely presence of hydrogen bubbles, which act as local high-pressure sites.

Hydrate Formation during the Compaction Stage. We discuss the results of two experiments in which hydrates were allowed to compact after formation. It was seen that the gas consumption rate during hydrate compaction is significantly lower than that during constant flow. A total of only 4.1 and 3.9 g of CO_2 was absorbed into the water (as hydrate or dissolved gas) over compaction times of 21.6 and 31.5 h, respectively. In contrast, 24.4, 24.9, and 24.1 g of CO_2 were captured by water over a flow time of t_{tot} = 14 min (pressurization + constant flow), suggesting a 2% repeatability error for 99% confidence. For the cases shown in Figure 2b, the gas consumption rate during constant flow is 199.5 ± 5.9 g h^{-1}, while that during compaction

https://doi.org/10.1021/acssuschemeng.4c03809
ACS Sustainable Chem. Eng. XXXX, XXX, XXX−XXX

is 0.16 ± 0.03 g h^{-1}. The 1275 times enhancement in the gas consumption rate highlights the advantages of a flow-based system for hydrate formation.

Relative Importance of Various Parameters on Hydrate Formation. Finally, we compare the influence of different parameters on the enhancement of hydrate formation. In order to compare on a normalized nondimensional basis, the fractional change in the sequestration rate with respect to the fractional change in the parameter under consideration was evaluated (Figure 6). Parameters considered include the

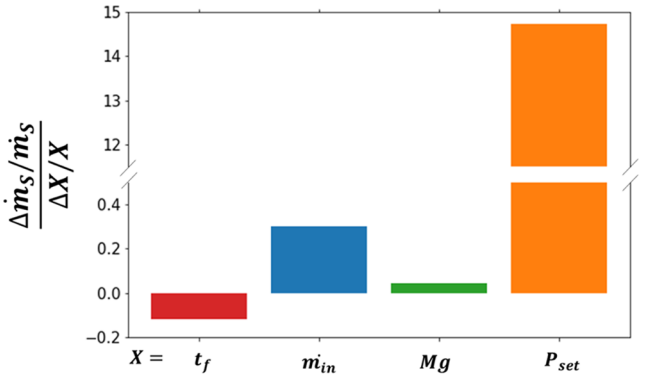

Figure 6. Relative influence of various parameters on the hydrate formation. The figure shows the fractional change in the sequestration rate per fractional change in experimental parameters, including formation time (t_f), gas flow rate ($\dot{m}_{in}$), amount of magnesium, and operating pressure (P_{set}).

formation time, inlet gas flow rate, amount of magnesium used, and operating pressure. It was observed that the most influential parameter was pressure, with a 14.7 times increase in sequestration rate seen per unit pressure change. Increasing the gas flow rate and amount of magnesium increased the sequestration rate but with much lower sensitivity, with a relative change of only 0.3 and 0.04, respectively. While this suggests that the amount of magnesium is not important, the presence of magnesium is critical for hydrate formation to occur (Table 2). Similarly, adequate flow rates are needed for mass and heat transfer enhancement. The combination of magnesium and the high CO_2 flow rate in an open system at high pressure is the recipe for maximizing foam formation rates. Longer formation times do reduce the sequestration rate (as should be expected), but not significantly (relative change of −0.12). Overall, this combination of variables can yield high sequestration rates for significant amounts of time. It should be noted that working with pressures higher than 3.55 MPa will entail risks of liquid CO_2 formation; this was indeed observed in our experiments, and such conditions were avoided. While hydrates can form from liquid CO_2 and water, the phenomena governing hydrate formation will be different from hydrate formation from gas−water mixtures.

CONCLUSIONS

Ultrafast formation of CO_2 hydrates using pure CO_2 is achieved without using any conventional chemical promoters or mechanical stirring. The key advancement is magnesium-induced promotion under high flow rate CO_2 sparging in an open system. The gas sequestration rate (in the form of a hydrate foam) remains constant over the duration of flow, suggesting the scalability of the approach. The sequestration rate is more sensitive to the reactor pressure than the gas flow rate or the amount of magnesium. Increasing the reactor pressure by 25%, from 2.86 MPa (400 psig) to 3.55 MPa (500 psig), increased the sequestration rate by 8×. A 3× increase in gas flow rate resulted in a 1.6× increase in sequestration rate and a decrease in CO_2 conversion fraction from 25.9 to 15.6%. Increasing the amount of magnesium by 6× resulted in an 18% higher sequestration rate. We have also established that ultrapure water is not an essential requirement for rapid hydrate formation, as similar sequestration rates (within 10%) were achieved with tapwater and deionized water. Our best results achieved a sequestration rate of 1276.5 g h^{-1} L^{-1} MPa^{-1}, which is >6× times higher than the state-of-the-art. Assuming that these results can be scaled up by maintaining the same rate of gas flow per unit volume of the reactor, these numbers imply that only 5 bubble column reactors of volume 10 m^3 are sufficient to sequester 1 Megaton/yr CO_2, which is the capacity of a typical injection project.[3] This highlights the promise of hydrate-based sequestration technologies toward meeting future gigascale sequestration requirements.

ASSOCIATED CONTENT

Supporting Information

The Supporting Information is available free of charge at https://pubs.acs.org/doi/10.1021/acssuschemeng.4c03809.

Nomenclature; model result highlighting the importance of high gas flow rate on hydrate formation; simulation results showing CO_2 sequestration rate as a function of gas flow rate and mole fraction of CO_2 in the gas; influence of formation time on (a) mass fractions of CO_2 within the reactor, and (b) relevant volume fractions in the reactor; detailed framework for analysis of hydrate formation in the reactor (PDF)

Hydrate formation with deionized (DI) water 3 (Video 1) (MP4)

Formation of hydrate shells and compaction 4 (Video 2) (MP4)

Hydrate formation with saltwater at 2.86 MPa (400 psig) 5 (Video 3) (MP4)

Dropping magnesium to trigger instantaneous hydrate formation with DI water (Video 4) (MP4)

AUTHOR INFORMATION

Corresponding Author

Vaibhav Bahadur − *Walker Department of Mechanical Engineering, The University of Texas at Austin, Austin, Texas 78751, United States;* orcid.org/0000-0001-7442-7769; Email: vb@austin.utexas.edu

Authors

Awan Bhati − *Walker Department of Mechanical Engineering, The University of Texas at Austin, Austin, Texas 78751, United States*

Mark Hamalian − *Walker Department of Mechanical Engineering, The University of Texas at Austin, Austin, Texas 78751, United States*

Palash V. Acharya − *Walker Department of Mechanical Engineering, The University of Texas at Austin, Austin, Texas 78751, United States*

Complete contact information is available at: https://pubs.acs.org/10.1021/acssuschemeng.4c03809

Author Contributions

A.B. conceived the idea of high flow rate continuous-flow sparging for rapid hydrate formation. A.B., P.A., and V.B. conceived the overall concept for this study. A.B. and V.B. planned out the experiments and analysis. A.B. assembled the experimental setup and conducted experiments and data analysis. M.H. assisted with experimentation. V.B. supervised the entire project and manuscript preparation.

Notes

The authors declare the following competing financial interest(s): The University of Texas at Austin has filed for two patents related to the research disclosed in this article.

■ ACKNOWLEDGMENTS

This study was supported by NSF grants 2234604, 1653412, and 2202071, along with support from the Energy Institute at UT Austin. Mark Hamalian acknowledges the NSF Graduate Fellowship.

■ ABBREVIATIONS

CCS, carbon capture and sequestration; BCR, bubble column reactor

■ REFERENCES

(1) Energy Technology Perspectives 2020 - Special Report on Carbon Capture Utilisation and Storage. 2020 DOI: 10.1787/208b66f4-en.
(2) XPRIZE. XPRIZE Carbon Removal Competition Rules & Guidelines 2023 https://www.xprize.org/. (Accessed May 23, 2024).
(3) Bhati, A.; Lokanathan, M.; Smaha, S.; Bahadur, V. Interviews of Industry Professionals as part of NSF I-Corps Program. 2022.
(4) Class VI Wells Permitted by EPA 2023 https://www.epa.gov/uic/class-vi-wells-permitted-epa. (Accessed May 23, 2024).
(5) Anchondo, C. Texas wants oversight of CO2 wells. Other states may follow Energy Wire 2022 https://www.eenews.net/articles/texas-wants-oversight-of-co2-wells-other-states-may-follow/. (Accessed May 23, 2024).
(6) Zheng, J.; Chong, Z. R.; Qureshi, M. F.; Linga, P. Carbon Dioxide Sequestration via Gas Hydrates: A Potential Pathway toward Decarbonization. *Energy Fuels* **2020**, *34* (9), 10529−10546.
(7) Shukla, R.; Ranjith, P.; Haque, A.; Choi, X. A review of studies on CO2 sequestration and caprock integrity. *Fuel* **2010**, *89* (10), 2651−2664.
(8) Lackner, K. S. A guide to CO2 sequestration. *Science* **2003**, *300*, 1677−1678.
(9) Voormeij, D.; Simandl, G. J. Geological, Ocean, and Mineral CO2 Sequestration Options: a Technical Review. *Geosci. Can.* **2004**, *31* (1), 11−22.
(10) Hu, G.; Li, Y.; Ye, C.; Liu, L.; Chen, X. Engineering Microorganisms for Enhanced CO 2 Sequestration. *Trends Biotechnol.* **2019**, *37* (5), 532−547.
(11) Winnefeld, F.; Leemann, A.; German, A.; Lothenbach, B. CO2 storage in cement and concrete by mineral carbonation. *Curr. Opin. Green Sustainable Chem.* **2022**, *38*, No. 100672.
(12) Alper, E.; Orhan, O. Y. CO2 utilization: Developments in conversion processes. *Petroleum* **2017**, *3* (1), 109−126.
(13) Acharya, P. V.; Kar, A.; Shahriari, A.; Bhati, A.; Mhadeshwar, A.; Bahadur, V. Aluminum-Based Promotion of Nucleation of Carbon Dioxide Hydrates. *J. Phys. Chem. Lett.* **2020**, *11* (4), 1477−1482.
(14) Kar, A.; Acharya, P. V.; Bhati, A.; et al. Magnesium-Promoted Rapid Nucleation of Carbon Dioxide Hydrates. *ACS Sustainable Chem. Eng.* **2021**, *9* (33), 11137−11146.
(15) IEA GHG. Gas Hydrates for Deep Ocean Storage of Co2 - Hydrates for Transportation and Deep Ocean Storage of Co2 - Background to the Study *IEA Greenh. Gas R&D Program. Rep. PH4/26* 2004.
(16) Linga, P.; Daraboina, N.; Ripmeester, J. A.; Englezos, P. Enhanced rate of gas hydrate formation in a fixed bed column filled with sand compared to a stirred vessel. *Chem. Eng. Sci.* **2012**, *68* (1), 617−623.
(17) Qureshi, M. F.; Zheng, J.; Khandelwal, H.; et al. Laboratory demonstration of the stability of CO2 hydrates in deep-oceanic sediments. *Chem. Eng. J.* **2022**, *432*, No. 134290.
(18) Tsouris, C.; Szymcek, P.; Taboada-Serrano, P.; McCallum, S. D.; et al. Scaled-Up Ocean Injection of CO 2 − Hydrate Composite Particles. *Energy Fuels* **2008**, *21* (4), 3300−3309.
(19) Riestenberg, D. E.; Tsouris, C.; Brewer, P. G.; et al. Field studies on the formation of sinking CO2 particles for ocean carbon sequestration: Effects of injector geometry on particle density and dissolution rate and model simulation of plume behavior. *Environ. Sci. Technol.* **2005**, *39* (18), 7287−7293.
(20) Kamath, V. A.; Holder, G. D. Dissociation heat transfer characteristics of methane hydrates. *AIChE J.* **1987**, *33* (2), 347−350.
(21) Golombok, M.; Ineke, E.; Luzardo, J. C. R.; He, Y. Y.; Zitha, P. Resolving CO2 and methane hydrate formation kinetics. *Environ. Chem. Lett.* **2009**, *7* (4), 325−330.
(22) Kar, A.; Bhati, A.; Acharya, P. V.; et al. Diffusion-based modeling of film growth of hydrates on gas-liquid interfaces. *Chem. Eng. Sci.* **2021**, *234*, No. 116456.
(23) Shahriari, A.; Acharya, P. V.; Carpenter, K.; Bahadur, V. Metal-Foam-Based Ultrafast Electronucleation of Hydrates at Low Voltages. *Langmuir* **2017**, *33* (23), 5652−5656.
(24) Acharya, P. V.; Shahriari, A.; Lin, D.; Bahadur, V. In *Mechanisms Underlying Rapid Electronucleation and Freezing of Hydrates*, ASME International Mechanical Engineering Congress and Exposition; ASME, 2017.
(25) Zheng, J.; Bhatnagar, K.; Khurana, M.; Zhang, P.; Zhang, B. Y.; Linga, P. Semiclathrate based CO2 capture from fuel gas mixture at ambient temperature: Effect of concentrations of tetra-n-butylammonium fluoride (TBAF) and kinetic additives. *Appl. Energy* **2018**, *217*, 377−389.
(26) He, J.; Liu, Y.; Ma, Z.; Deng, S.; Zhao, R.; Zhao, L. A Literature Research on the Performance Evaluation of Hydrate-based CO2 Capture and Separation Process. *Energy Procedia* **2017**, *105*, 4090−4097.
(27) Li, A.; Jiang, L.; Tang, S. An experimental study on carbon dioxide hydrate formation using a gas-inducing agitated reactor. *Energy* **2017**, *134*, 629−637.
(28) Li, G.; Liu, D.; Xie, Y.; Xiao, Y. Study on effect factors for CO2 hydrate rapid formation in a water-spraying apparatus. *Energy Fuels* **2010**, *24* (8), 4590−4597.
(29) Linga, P.; Kumar, R.; Dong, J.; Ripmeester, J.; Englezos, P. A new apparatus to enhance the rate of gas hydrate formation: Application to capture of carbon dioxide. *Int. J. Greenhouse Gas Control* **2010**, *4*, 630−637.
(30) Kumar, A.; Sakpal, T.; Linga, P.; Kumar, R. Enhanced carbon dioxide hydrate formation kinetics in a fixed bed reactor filled with metallic packing. *Chem. Eng. Sci.* **2015**, *122*, 78−85.
(31) Gaikwad, N.; Bhattacharjee, G.; Kushwaha, O. S.; Sangwai, J. S.; Linga, P.; Kumar, R. Effect of Cyclooctane and l -Tryptophan on Hydrate Formation from an Equimolar CO2-CH4Gas Mixture Employing a Horizontal-Tray Packed Bed Reactor. *Energy Fuels* **2020**, *34* (8), 9840−9851.
(32) Gaikwad, N.; Bhattacharjee, G.; Sangwai, J. S.; Kumar, R.; Linga, P. Kinetic and Morphology Study of Equimolar CO2-CH4Hydrate Formation in the Presence of Cyclooctane and l -Tryptophan. *Energy Fuels* **2021**, *35* (1), 636−648.
(33) Sahu, C.; Sircar, A.; Sangwai, J. S.; Kumar, R. Effect of Methylamine, Amylamine, and Decylamine on the Formation and Dissociation Kinetics of CO2Hydrate Relevant for Carbon Dioxide Sequestration. *Ind. Eng. Chem. Res.* **2022**, *61* (7), 2672−2684.
(34) Linga, P.; Kumar, R.; Englezos, P. Gas hydrate formation from hydrogen/carbon dioxide and nitrogen/carbon dioxide gas mixtures. *Chem. Eng. Sci.* **2007**, *62* (16), 4268−4276.

(35) Zhou, S. D.; Yu, Y. S.; Zhao, M. M.; Wang, S. L.; Zhang, G. Z. Effect of graphite nanoparticles on promoting CO2 hydrate formation. *Energy Fuels* **2014**, *28* (7), 4694−4698.
(36) Xu, C. G.; Li, X. S.; Lv, Q. N.; Chen, Z. Y.; Cai, J. Hydrate-based CO2 (carbon dioxide) capture from IGCC (integrated gasification combined cycle) synthesis gas using bubble method with a set of visual equipment. *Energy* **2012**, *44* (1), 358−366.
(37) Chen, Z.; Fang, J.; Xu, C.; Xia, Z.; Yan, K.; Li, X. Carbon dioxide hydrate separation from Integrated Gasification Combined Cycle (IGCC) syngas by a novel hydrate heat-mass coupling method. *Energy* **2020**, *199*, No. 117420.
(38) Nasir, Q.; Suleman, H.; Elsheikh, Y. A. A review on the role and impact of various additives as promoters/ inhibitors for gas hydrate formation. *J. Nat. Gas Sci. Eng.* **2020**, *76*, No. 103211.
(39) Kar, A.; Bahadur, V. Analysis of coupled heat & mass transfer during gas hydrate formation in bubble column reactors. *Chem. Eng. J.* **2023**, *452*, No. 139322.
(40) Ramachandran, N.; Aboudheir, A.; Idem, R.; Tontiwachwuthikul, P. Kinetics of the absorption of CO2 into mixed aqueous loaded solutions of monoethanolamine and methyldiethanolamine. *Ind. Eng. Chem. Res.* **2006**, *45* (8), 2608−2616.
(41) Kumar, A.; Palodkar, A. V.; Gautam, R.; Choudhary, N.; Veluswamy, H. P.; Kumar, S. Role of salinity in clathrate hydrate based processes. *J. Nat. Gas Sci. Eng.* **2022**, *108*, No. 104811.

https://doi.org/10.1021/acssuschemeng.4c03809
ACS Sustainable Chem. Eng. XXXX, XXX, XXX−XXX